2016 Report

Single-unit dynamics in the epileptic foci in patients with temporal lobe epilepsy

EPIDYN

PN-II-ID-PCE-2011-3-0240

Contract 153/2011

Objectives

The main objective of our studies is to acquire a better understanding of the mechanisms underlying seizure generation and its propagation across various brain areas in patients with drug-resistant epilepsy.

In an attempt to understand the **single-unit signature of pathological cortex**, we probe the susceptibility to synchronization of epileptogenic tissue by recording single-unit response to intraoperative electrical stimulation applied to the seizure onset zone (SOZ) in patients undergoing resective surgery for drug-resistant epilepsy.

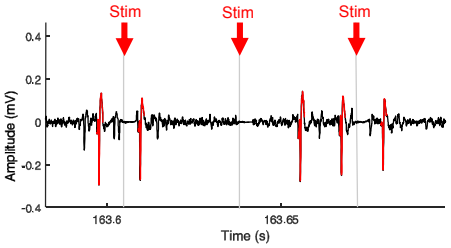

We aim at understanding the **propagation pathways of the pathological activity** by studying the intracranial EEG responses to single-pulse electrical stimulation and calculating a **whole-brain effective connectome**.

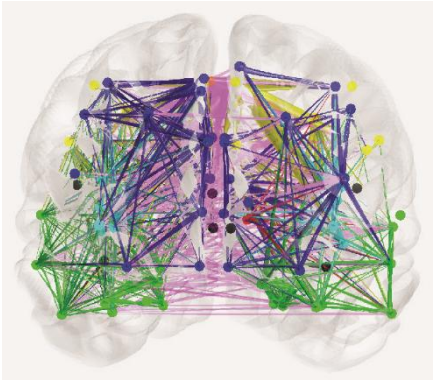

Single-unit activity

Patients and Methods

We have recorded single-unit activity in 12 patients with drug-resistant focal epilepsy undergoing SEEG presurgical evaluation (Barborica et al, 2015).

Patient	Sex	Age	Pathology	Epilepsy	SOZ
1	F	32	Type I FCD	Temporal	Mesial structures
2	M	46	Sclerosis	Mesio-temporal	Amygdala
3	M	39	MCD	Temporo-occipital	Basal
4	M	47	DNET	Temporal	Middle temporal gyrus
5	F	40	Type II B FCD	Prefrontal	Dorsolateral prefrontal cortex
6	F	35	Gliosis	Mesio-temporal	Amygdala
7	F	25	Type II FCD	Temporal	Temporal pole
8	F	46	Type II FCD	Temporal	Temporal pole
9	M	33	Type I FCD	Frontal	Anterior cingulate cortex
10	M	28	Type I FCD	Temporal	Hippocampus
11	F	25	Type I FCD	Temporal	Entorhinal cortex
12	M	53	Cavernoma	Frontal	Frontal pole

Prior to the resective surgery, we are stereotactically inserting three microelectrodes, spaced 2mm apart, in a linear configuration, following a trajectory targeting SOZ.

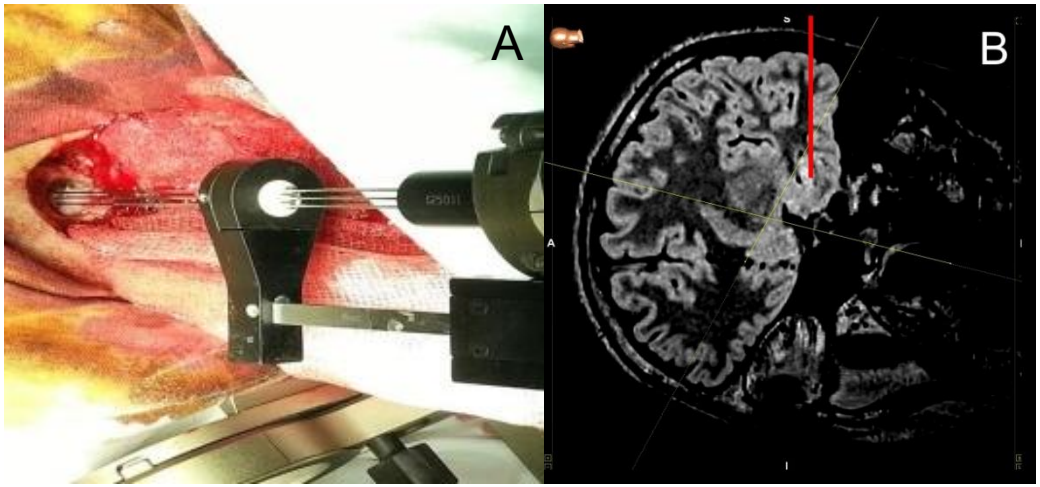

Figure 1. A) Acute microelectrode recording setup using clinical microelectrodes; B) Electrode trajectory in patient 10, shown in red, passing through several sulci in temporo-basal epileptogenic cortex and targeting the hippocampus, which is the seizure onset zone.

Bipolar electrical stimulation is applied in most cases between the two outer macro contacts of the electrodes, while recording the unit activity on the center microelectrode, located 3 mm deeper than the macro contacts. Constant current 0.5 to 1 mA biphasic pulses, 0.3 ms pulse width, frequency 1, 10, 30, 60 were applied for 30 s using a clinical recording and stimulating system (Guideline LP+, FHC Inc, Bowdoin, ME). The interval before, between and after each electrical stimulation epoch was at least 30 seconds.

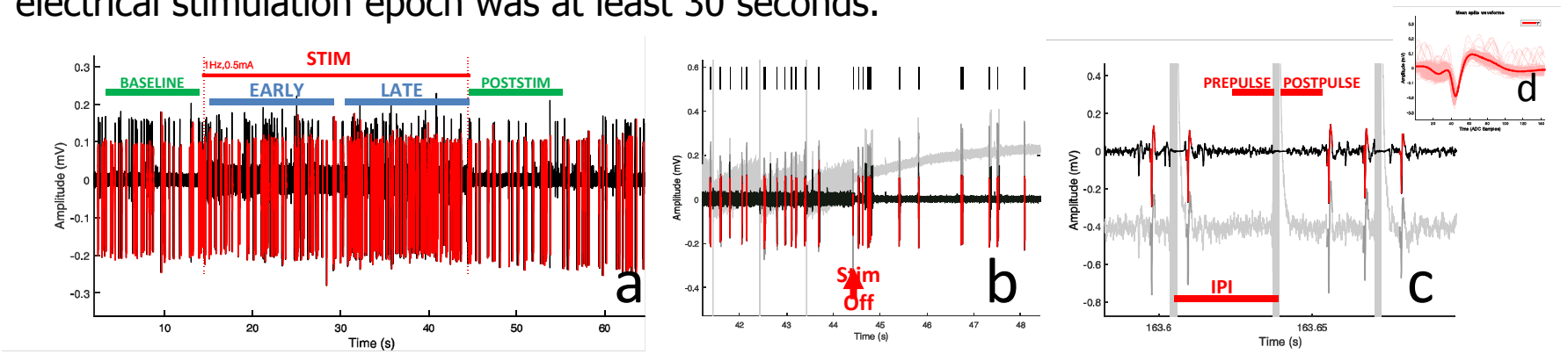

Figure 2. Illustration of the recording while stimulating, stimulus artifact removal and spike discrimination. a) the 1-Hz stimulation epoch recorded in patient 7 with discriminated neurons highlighted in red; b) a detail of the end of the stimulation epoch, showing the raw signal (gray) and the filtered signal. c) example of neurons recovered from the 30-Hz stimulation epoch. The blanking interval is 4.16 ms, accounting for 4.16% of the inter-pulse interval at 10 Hz and 25% at 60 Hz. d) mean spike waveform of the neuron presented in a), b) and c).

Firing rate modulation indexes were calculated for a) assessing the effect of electrical stimulation, defined as the difference between mean firing rate during stimulation and the pre-stimulation baseline, divided by the sum of the two; b) assessing the time course of the stimulation, defined like the previous index, but using the early and late responses during each stimulation epoch

$$MI_{STIM} = \frac{R_{STIM} - R_{BASELINE}}{R_{STIM} + R_{BASELINE}} \qquad MI_{BUILDUP} = \frac{R_{LATE} - R_{EARLY}}{R_{LATE} + R_{EARLY}} \qquad TLI = \frac{R_{POSTPULSE} - R_{PREPULSE}}{R_{POSTPULSE} + R_{PREPULSE}}$$

Results

Firing activity is time-locked to the stimulus. The time-locking is frequency dependent, as illustrated in Fig. 3.

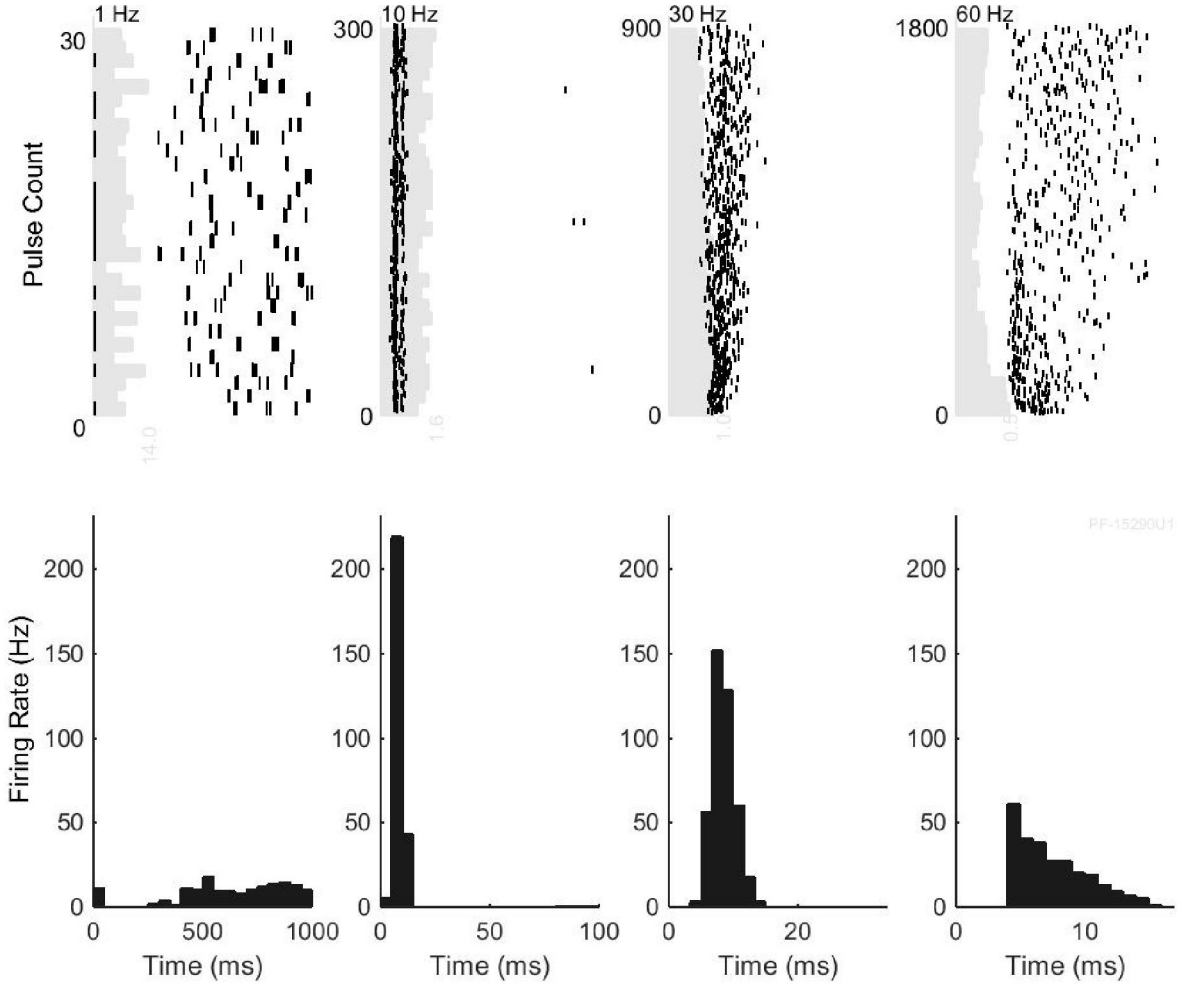

Figure 3. Peri-stimuls histograms (bottom row) and rasters (top row) of a neuron in patient 3. The time-locking index takes values of -48.9%, 98.2%, 100%, and 53.2% for the 1, 10, 30 and 60 Hz stimulation frequencies, respectively. The light gray histograms behind the rasters illustrate the variation of the spike count per stimulation cycle.

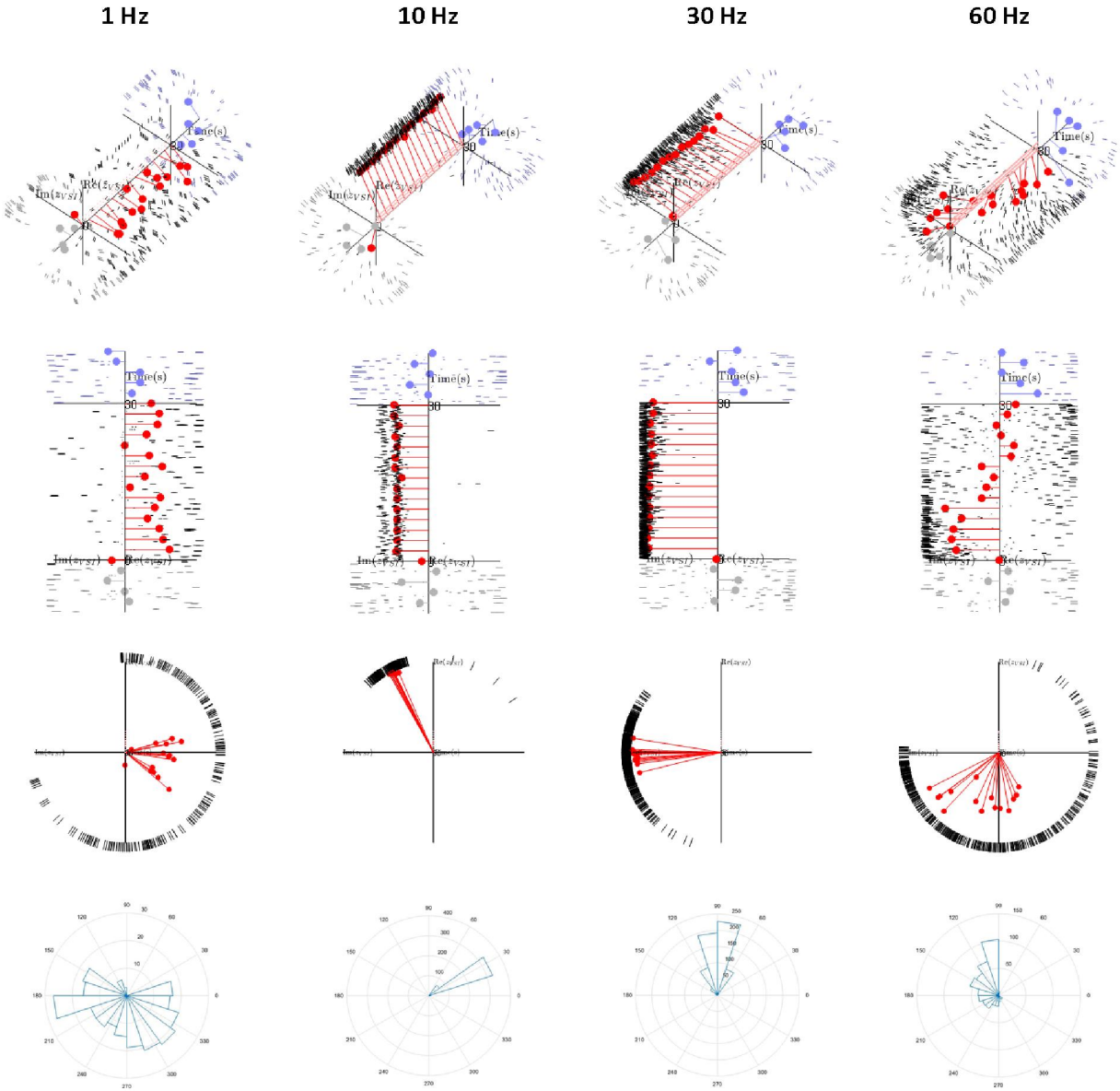

Figure 4. A representation of the firing in complex plane has been performed by introducing a complex representation of the spikes: $z_i = \cos(2\pi f_s t_i) + j\sin(2\pi f_s t_i)$, where f_s is the stimulation frequency and t_i is the spike time, relative to the stimulation pulse. The 3D representation of the complex spikes for 1, 10, 30 and 60 Hz stimulation, calculated over 2 sec bins. Phase histograms of the action potentials are shown on the last row.

At the population level, a 3-way Anova analysis of the firing rate (MI_{STIM}, $MI_{BUILDUP}$) showed a significant dependence on the patient ($p<0.05$) but non-significant dependence on frequency and epileptogenicity ($p>0.1$). By contrast, **time-locking (*TLI*) depended significantly on all factors**: patient ($p<0.001$), epileptogenicity ($p<0.05$), and frequency ($p<0.01$).

	Epileptogenicity	All frequencies	1 Hz	10 Hz	30 Hz	60 Hz
MI_{STIM}	All neurons	0.10±0.49, n=81	0.13±0.50, n=21	-0.02±0.38, n=21	0.20±0.54, n=21	0.07±0.55, n=18
	EZ	0.10±0.51, n=58	0.12±0.50, n=15	-0.08±0.35, n=15	0.20±0.57, n=15	0.15±0.61, n=13
	non-EZ	0.09±0.46, n=23	0.16±0.54, n=6	0.11±0.46, n=6	0.19±0.50, n=6	-0.14±0.33, n=5
$MI_{BUILDUP}$	All neurons	-0.09±0.37, n=81	0.03±0.37, n=21	-0.08±0.29, n=21	-0.16±0.25, n=21	-0.17±0.54, n=18
	EZ	-0.13±0.40, n=58	-0.01±0.33, n=15	-0.13±0.30, n=15	-0.16±0.27, n=15	-0.25±0.62, n=13
	non-EZ	0.02±0.30, n=23	0.15±0.47, n=6	0.05±0.21, n=6	-0.15±0.22, n=6	0.01±0.18, n=5
TLI	All neurons	0.15±0.42, n=81	-0.10±0.25, n=21	0.25±0.51, n=21	0.26±0.45, n=21	0.20±0.29, n=18
	EZ	0.21±0.48, n=58	-0.13±0.28, n=15	0.33±0.59, n=15	0.36±0.50, n=15	0.28±0.29, n=13
	non-EZ	0.01±0.11, n=23	-0.02±0.11, n=6	0.05±0.05, n=6	0.03±0.13, n=6	-0.03±0.15, n=5

Table 2. Firing rate modulation index due to the application of electrical stimulation, activity buildup index during stimulation epoch and time-locking to stimulation pulses index. The number n of trials or neurons in each category are listed along with mean±SD index values.

Single-unit Study

Conclusions

- Our study at the microscale shows that susceptibility to hypersynchronization of neurons in epileptogenic cortex can be probed with electrical stimulation.
- There is a strong frequency-dependence of the effects, as stimulation pulses with low repetition rate generally fail to entrain neural activity.
- Time-locking, but not firing rate, correlates with tissue epileptogenicity.
- **Susceptibility for time locking to stimulation pulses may therefore be considered as a single-unit signature of the pathological cortex.**

Effective Connectome

We propose a method, as described in Donos et al., 2016a, that allows us to study the effective brain connectivity, referring to the influence one area of the brain exerts over another (Friston, 1994), in a large number of brain structures, using single-pulse electrical stimulation. The effective connectivity is combined with the anatomical information about white matter tracts, obtained from a DSI atlas, to form a physiological structural-effective connectome (SEC) (Fig. 1a)

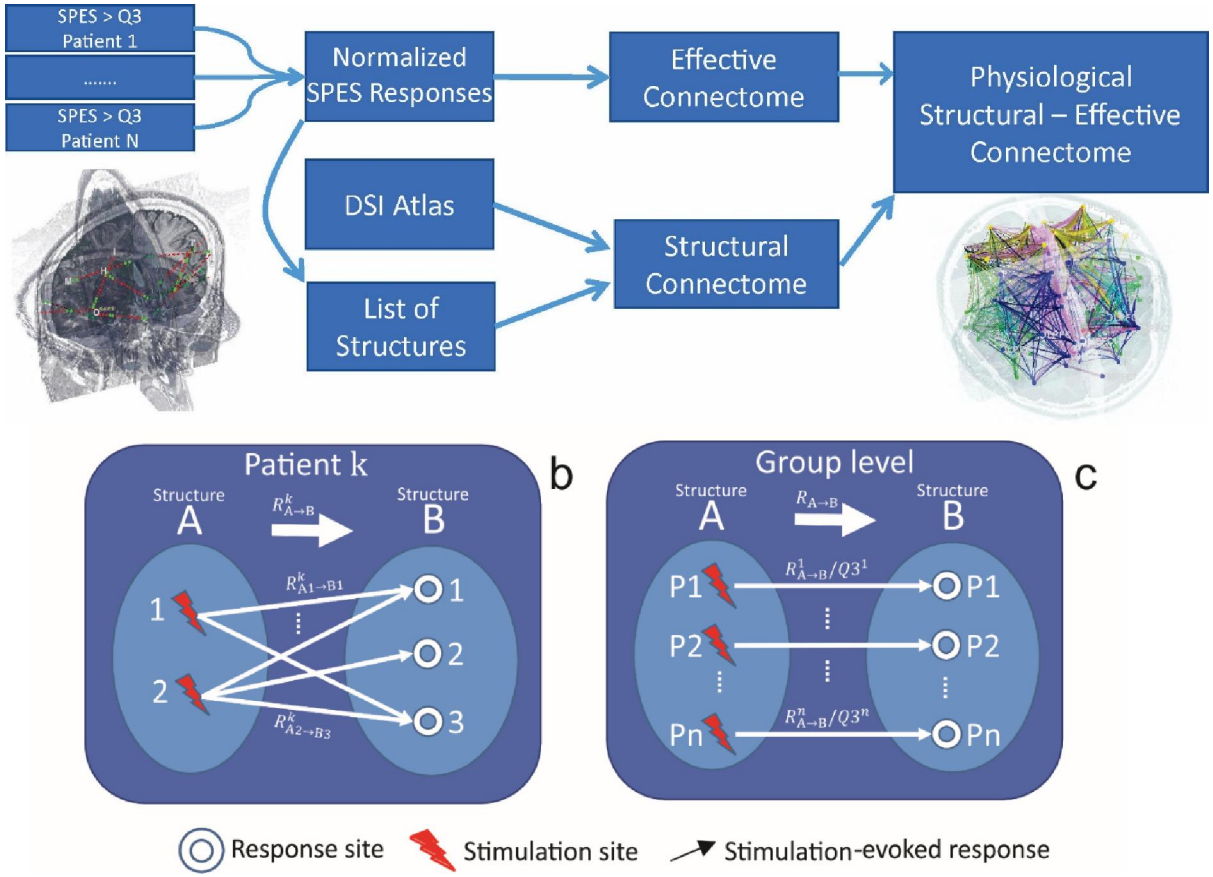

Figure 5. a) The workflow for obtaining a physiological structural-effective connectome; b) A detail of the workflow used for calculating the effective connectivity $R^{k}_{A\rightarrow B}$ between two structures (A ,B) implanted with multiple contacts, at the patient-level; c) An illustration of the homogenization of patients' responses by normalization with the patient specific activation threshold (third quartile of the responses, $Q3^{n}$), before averaging across n patients.

Effective Connectome

Patients and Methods

We have recorded responses to single-pulse electrical stimulation in 24 patients with drug-resistant focal epilepsy undergoing SEEG presurgical.

Patient	Sex	Age	Epilepsy	Lateralization	Localization	Pathology	MRI Lesion	Number of electrodes	Number of contacts	RMS Q3 (uV)	Surgical Outcome
1	F	17	Frontal	Left	Premotor dorsolateral	Type II B FCD	Negative	11	104	95.8	Engel IIIB
2	M	39	Occipital	Left	Occipito-temporal basal	Polimycrogyria	MCD	16	194	61.3	Engel IA
3	M	47	Temporal	Left	Middle temporal gyrus	DNET	DNET	11	101	87.7	Engel II
4	F	40	Prefrontal	Left	Prefrontal	Type II B FCD	Type II B FCD	11	141	89.6	Engel IA
5	F	35	Mesio-temporal	Right	Amygdala	Temporal sclerosis	Negative	12	160	56.4	Engel IIB
6	F	24	Fronto-central	Right	Rolandic	Type II A FCD	Type II FCD	15	138	63.9	Engel IB
7	M	24	Occipital	Right	Occipito-temporal basal	Type I FCD	MCD	14	157	25.3	Engel IIIB
8	F	25	Temporal	Right	Amygdala	Type I FCD	Type II FCD	10	111	62.5	Engel IIB
9	F	46	Temporal	Right	Temporal pole	Type II B FCD	Type II FCD	9	102	106.5	Engel IIIB
10	M	33	Frontal	Left	Mesial prefrontal	Type I B FCD	Type I FCD	17	174	48.4	Engel IA
11	F	11	Frontal	Right	Mesial and lateral premotor	Type II A FCD	Misleading-type II B - like FCD in temporal operculum	9	183	77.7	Engel IA
12	F	9	Frontal	Right	Lateral prefrontal	Type II A FCD	Type II FCD	13	180	54.8	Engel IC
13	F	35	Frontal	Right	Middle cingulate	Not available (thermocoagulation)	Negative	14	169	48.2	Engel IA
14	M	28	Temporal	Right	Temporal	Type I FCD	Type I FCD	17	188	52.1	Engel IA
15	F	25	Bitemporal	Bilateral	Bitemporal	Type I FCD	Negative	17	219	51.8	Engel IB
16	F	36	Opercular	Right	Parietal-temporal, posterior operculum	Type II B FCD	Type II FCD	15	205	91.4	Engel IA
17	F	42	Temporal plus	Right	Temporal pole and temporo-mesial	Type I FCD	Hippocampal atrophy	14	205	72.1	Engel IA
18	F	37	Temporal	Left	Temporal pole and temporo-mesial	Type IIA FCD	Negative	13	160	43.6	Engel IA
19	M	26	Occipital	Bilateral	Bioccipital	Not operated on	Negative	14	211	73.3	-
20	M	53	Frontal	Left	Frontal pole	Cavernoma	Multiple cavernomas	11	166	30.2	Engel IA
21	M	39	Bitemporal	Bilateral	Bitemporal	Not operated on	Negative	11	167	44.9	-
22	F	42	Temporal	Left	Temporal	Not available	Hippocampal atrophy and left superior temporal gyrus malformation	11	147	58.8	Engel IA
23	M	42	Mesio-Temporal	Left	Occipito-temporo basal	Type II A FCD	Left hippocampal sclerosis and superior temporal gyrus dysplasia	14	194	65.2	Engel IB
24	M	29	Frontal	Right	Premotor	Type II B FCD	Type II B FCD	9	112	72	Engel IA

Table 3. Patients participating in the study. MCD – malformation of cortical development, DNET - dysembryoplastic neuroepithelial tumour, FCD – focal cortical dysplasia.

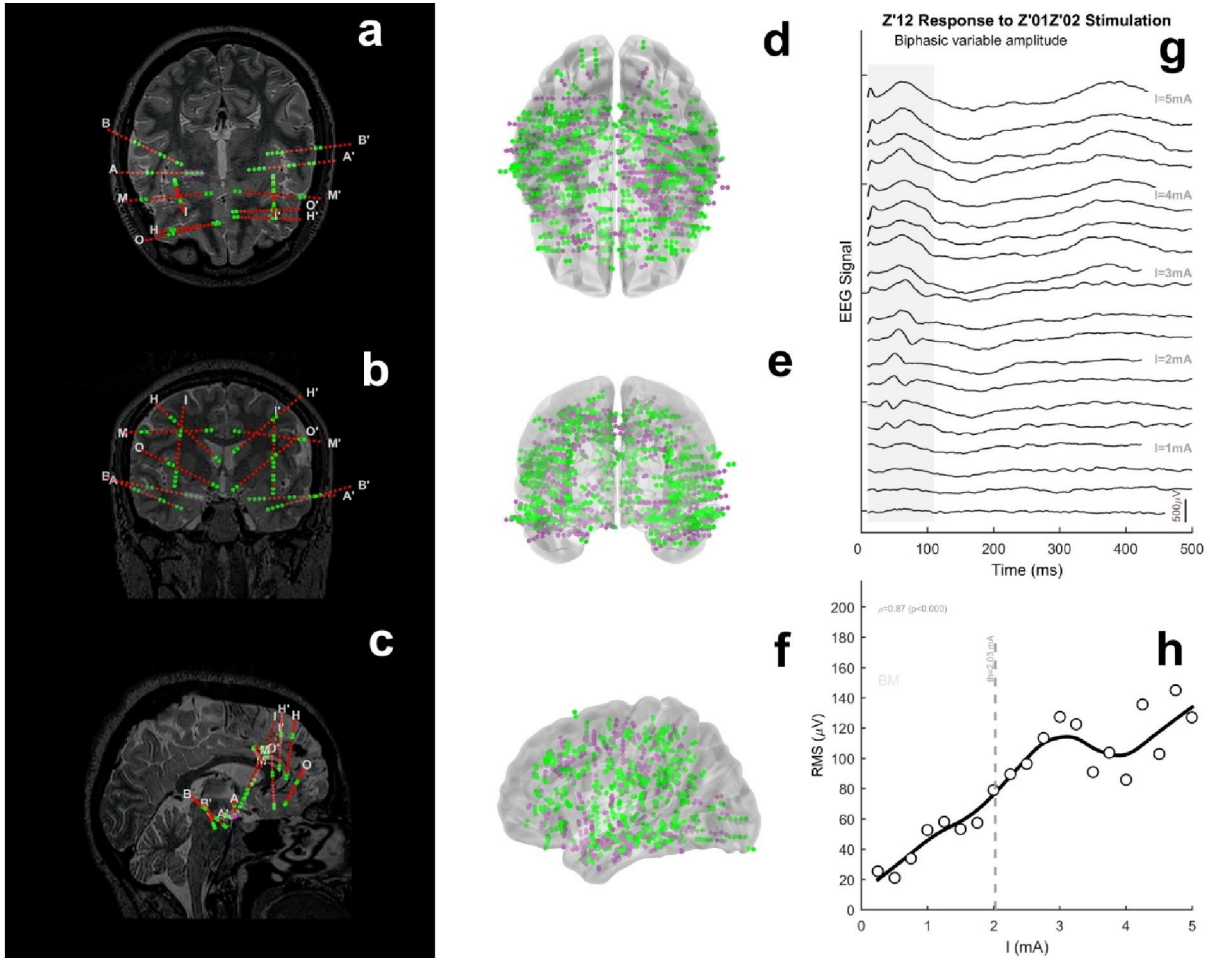

Figure 6. a-c): The implantation scheme of patient 5, showing the contacts used in the EEG montage colored in green, while unused contacts are colored in red; d-f): Pool of 1481 contacts implanted in 24 patients, 634 contacts located in the epileptogenic zone (magenta) and 847 outside the epileptogenic zone (green); g) stimulus-aligned EEG traces, sorted by the current amplitude, showing changes in the latency of a stimulation-evoked response, as a result of complex and variable morphology of the responses to pulses of different amplitudes in a stimulation trial; h) stimulus–response curve for the early response amplitude in the 10-110ms post-stimulation window, marked as a shaded area.

The first step in obtaining the effective connectome was to perform an average of the responses for multiple contacts located in the same structure, for each patient, using a workflow illustrated in Fig. 5. To assess the effective connectivity at the patient level, we first averaged the response amplitude for stimulated-recorded pairs of contacts belonging to the same pair of structures, using the following formula:

$$R^{k}_{A\to B} = \frac{\sum_{i}^{N_A}\sum_{j}^{N_B} R_{A_i\to B_j}}{N_{R_{AB}}}$$

where $R^{k}_{A\to B}$ is the effective connectivity measure (same units as the responses) between stimulated structure A and the structure B, where the responses are recorded, $R_{A_i\to B_j}$ is response recorded on contact *j* of structure B when stimulating site *i* of structure A, N_A and N_B are the number of stimulation and recording sites, respectively, NR_{AB} is the number of stimulation-evoked responses recorded in structure B when stimulating all sites from structure A

To calculate the group-level effective connectome (EC), we have normalized the connections of each patient-level effective connectome to the patient-specific activation threshold for each patient, as illustrated in Fig 2c, using the formula:

$$R_{\mathrm{A}\to\mathrm{B}} = \sum_{i=1}^{N} \frac{R_{A\to B}^{i}}{Q3^{i}}$$

where $R_{A\to B}$ is the effective connectivity measure between structures A and B averaged across N patients, $R_{A\to B}^{i}$ is the effective connectivity measure in patient *i*, and $Q3^{i}$ is the activation threshold of patient *i*.

The directionality of the connections between a pair of structures (A, B) is evidenced by the asymmetry in responses $R_{A\to B}$, $R_{B\to A}$ to sequential stimulation of each structure. A directionality factor $DF_{A\leftrightarrow B}$ has been defined as:

$$DF_{A\leftrightarrow B} = \left|\frac{R_{A\to B} - R_{B\to A}}{R_{A\to B} + R_{B\to A}}\right|$$

Normalized individual ECs and combined into the population level EC by averaging the connections available in the individual connectomes, on a structure-by-structure basis.

Abbrev.	Structure's name	Contacts		Patients		Abbrev.	Structure's name	Contacts		Patients	
		Right	Left	Right	Left			Right	Left	Right	Left
FRONTAL							**OPERCULAR-INSULAR**				
ACC	Anterior Cingulate Cortex	13	13	6	6	**aI**	Anterior Insula	8	2	5	1
DLPFC	Dorso-Lateral Prefrontal Cortex	24	5	5	3	**OpF**	Operculum Frontalis	5	6	3	3
DMPFC	Dorso-Mesial Prefrontal Cortex	4	8	2	3	**OpP**	Operculum Parietalis	17	10	4	4
MCC	Middle Cingulate Gyrus	8	2	3	1	**OpR**	Operculum Rolandis	9	2	4	1
MOFC	Mesial Orbito-Frontal Cortex	4	8	2	4	**OpT**	Operculum Temporalis	14	15	5	5
OF	Orbito-Frontal	10	8	4	4	**pI**	Posterior Insula	18	16	7	7
PMC	Premotor Cortex	24	9	6	2		**PARIETAL**				
preSMA	Pre-Supplementary Motor Area	3	1	2	1	**IPL**	Inferior Parietal Lobule	24	7	7	5
R	Precentral Gyrus	18	12	6	3	**PCC**	Posterior Cingulate Cortex	7	21	4	8
SMA	Supplementary Motor Area	4	2	2	1	**PCL**	Paracentral Lobule	12	6	4	3
VLPFC	Ventro-Lateral Prefrontal Cortex	4	11	2	3	**PrC**	Precuneus	6	12	3	4
VMPFC	Ventro-Mesial Prefrontal Cortex	0	2	0	1	**S**	Postcentral Gyrus	7	2	4	1
TEMPORAL						**SPL**	Superior Parietal Lobule	8	21	4	6
A	Amygdala	10	12	4	5		**OCCIPITAL**				
E	Entorhinal	0	4	0	2	**C**	Cuneus	2	0	1	0
F	Fusiform Gyrus	6	20	3	6	**LG**	Lingual Gyrus	17	13	6	5
Hc	Hippocampus	7	3	4	1	**O**	Lateral Occipital	3	5	2	1
ITG	Inferior Temporal Gyrus	20	21	9	7	**TPO**	Temporo-Parieto-Occipital Junction	16	4	6	1
MTG	Middle Temporal Gyrus	18	26	6	6	**V1**	Primary Visual Cortex	5	1	1	1
PHG	Parahippocampal Gyrus	4	19	2	4		**SUBCORTICAL**				
STG	Superior Temporal Gyrus	13	21	5	7	**BG**	Basal Ganglia (Putamen)	0	1	0	1
TP	Temporal Pole	3	6	2	2	**Th**	Thalamus (Anterior Nucleus and Pulvinar)	0	3	0	2

Table 4. List of structures implanted in our patient set.

The **structural connectome** (SC) was computed from the CMU-60 template, made freely available by The Cognitive Axon (CoAx) Lab (Department of Psychology, Carnegie Mellon University, http://www.psy.cmu.edu/~coaxlab). The template is based on an averaged map of reconstructed fiber orientations, obtained from 60 neurologically healthy volunteers that were scanned at the Scientific Imaging and Brain Research Center, Carnegie Mellon University (Yeh and Tseng 2011).

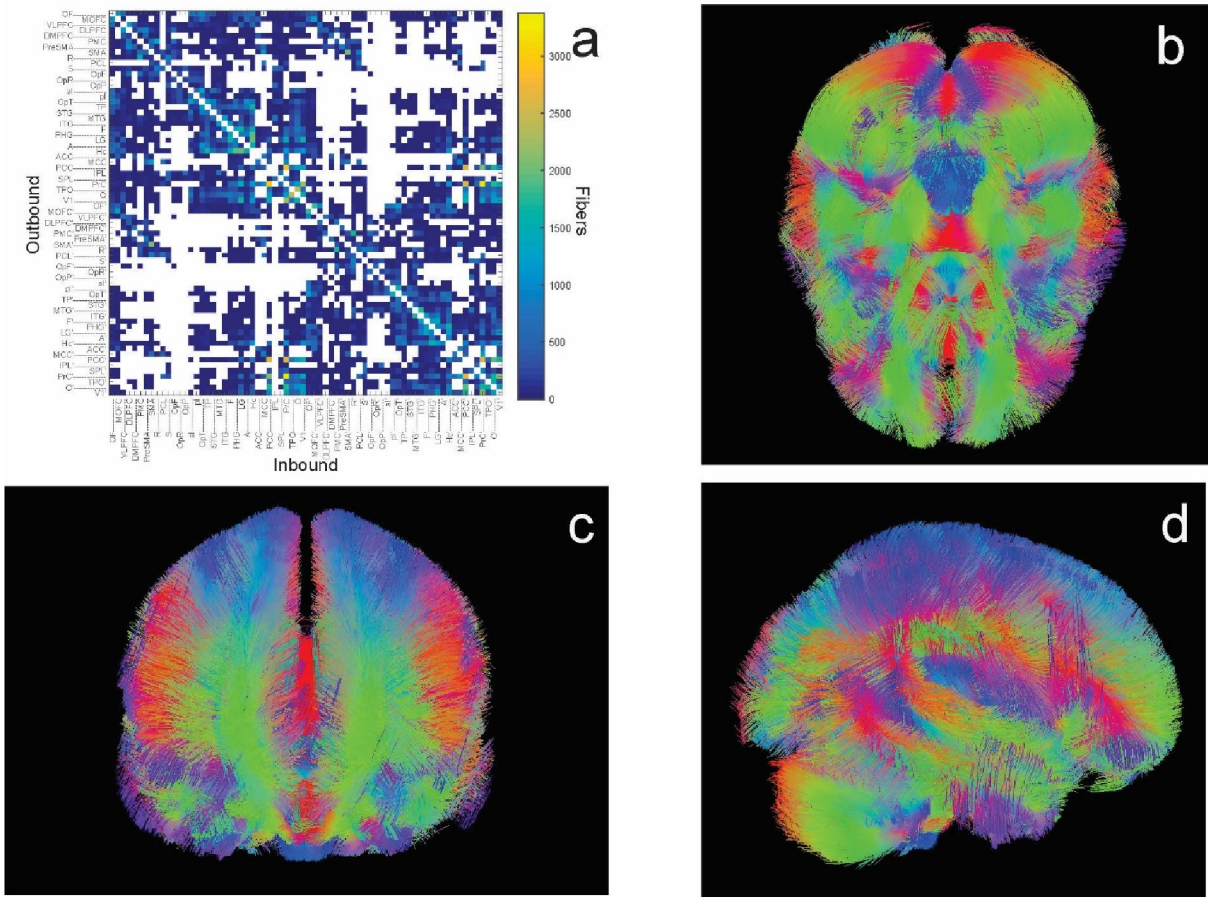

Figure 7. The Structural Connectome. a) 2D representation as an adjacency matrix, in which the number of tracts connecting two structures is color-coded. A white square marks the absence of fibers connecting the structures. b),c),d) Axial, coronal, and sagittal views of the 3D direction map.

Results

For the **EC**, the connections' strength is given by the magnitude of the responses evoked by SPES (Donos et al 2016a). For the 3D representation, we use a glass brain based on the MNI152 atlas where each brain structure is represented as a colored sphere and each causal connection as a conical frustum.

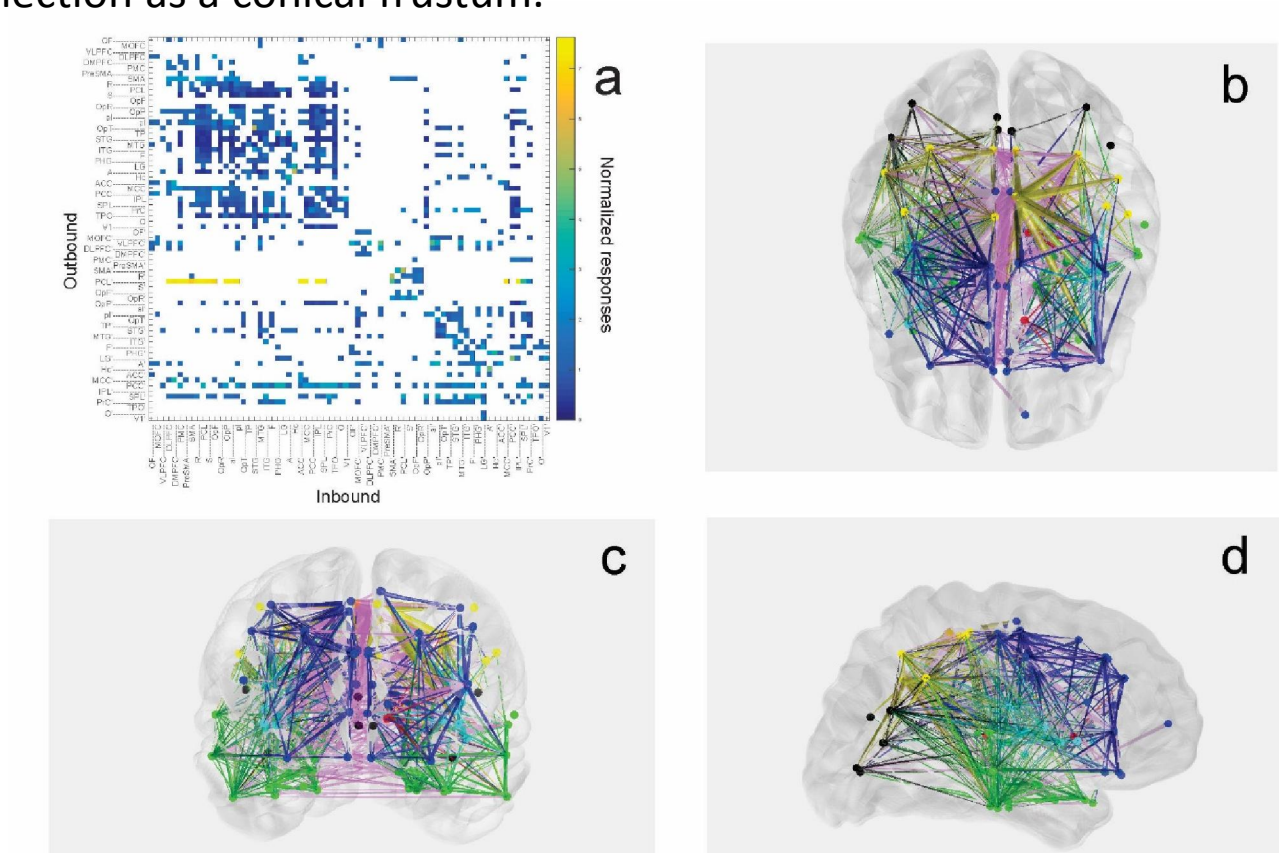

Figure 8. The Effective Connectome. a) 2D representation as an adjacency matrix, in which the normalized responses between two structures are color-coded. b),c),d) Axial, coronal, and sagittal views of the 3D frustums representation. For each connection, the large base of the frustum, whose radius is directly proportional to the normalized responses, indicates the stimulation structure, while the small base indicates the structure in which the response was recorded

By excluding the stimulations and responses in pathological structures, we obtain the physiological SEC that shows functionally active direct connections between the brain structures, whose connection strength is quantified by the effective number of fibers, EF, calculated as described in the methods section.

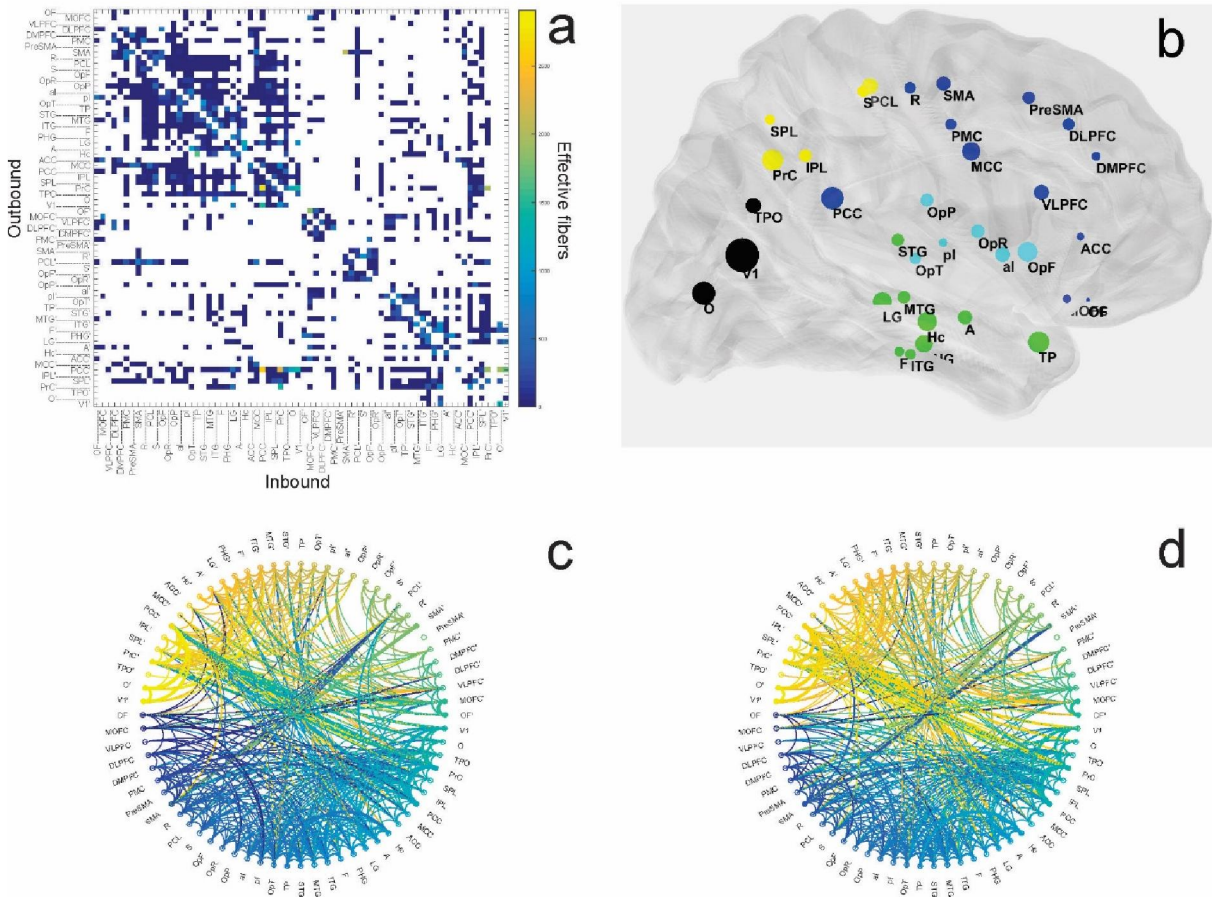

Figure 9. The Physiological Structural-Effective Connectome. a) 2D representation as an adjacency matrix, in the connection between two structures is quantified by the EF, color-coded. b) clustering coefficient distribution for the right hemisphere brain structures. The clustering coefficient value is directly proportional with the size of the colored spheres. Temporal lobe – green, parietal lobe – yellow, occipital lobe – black, frontal lobe – blue, opercular-insular – cyan. c) ,d) circular graph representations of the inbound and outbound physiological SEC, respectively. The EF is directly proportional with the width of each connection.

PSEC connectivity of individual structures

Inbound

Outbound

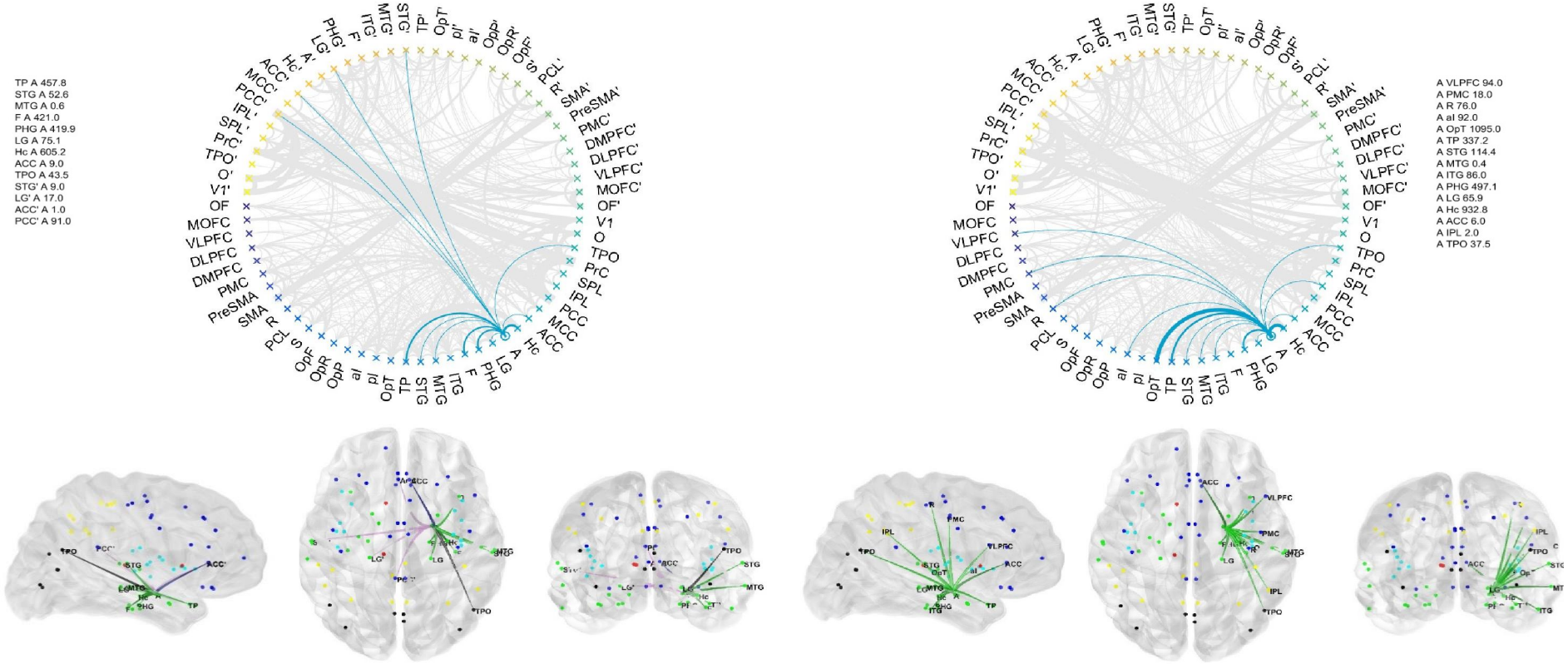

Figure 10. The Physiological Structural-Effective connectivity of the right Amygdala.

The pairwise correlation between the structural and effective connectomes has been assessed using Kendall's rank correlation coefficient, whose values ranging from -0.52 to 0.44 are represented in Fig. 11 with statistically significant correlations (p<0.05) marked with a star.

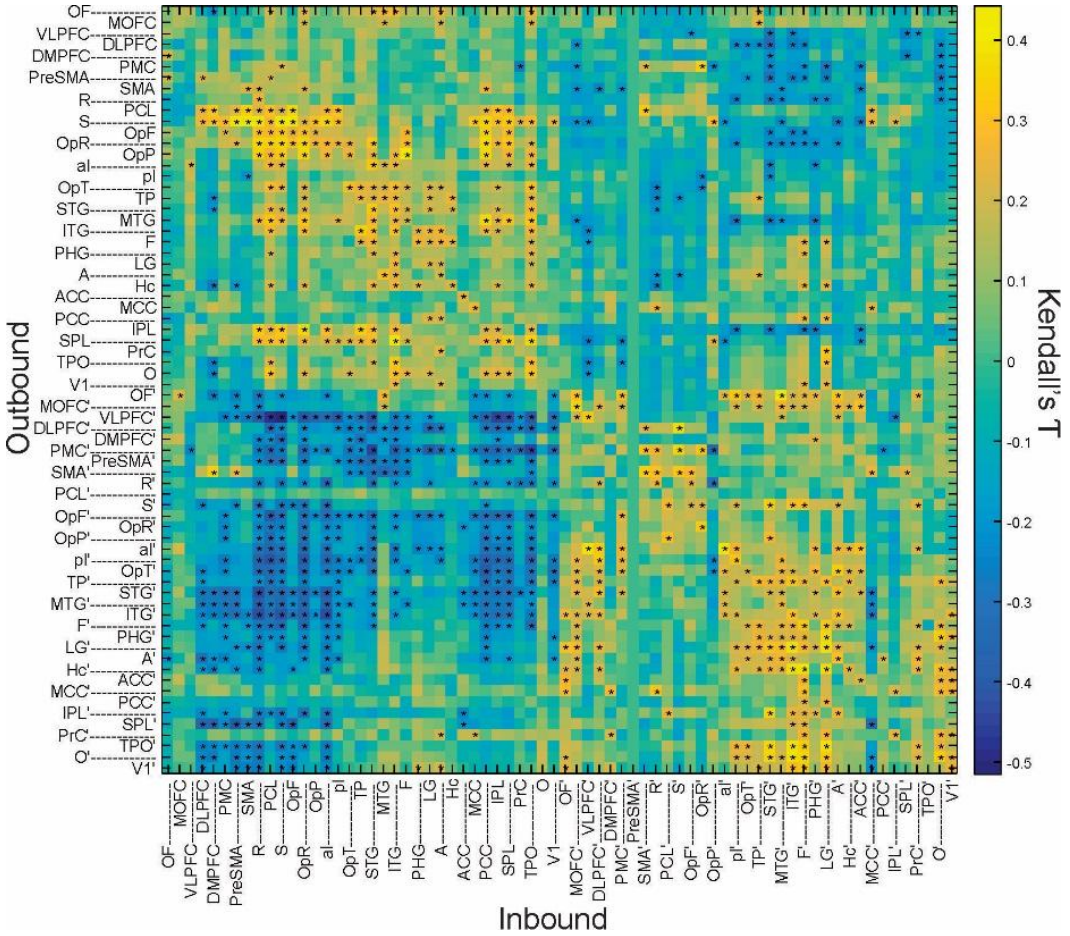

Figure 11. Correlation matrix between the structural and effective connectomes. Kendall's rank correlation coefficient is shown in color-code, with stars marking statistically significant correlations (p<0.05)

As not all structures are directly connected, the propagation pathways indirectly connecting various structures within the brain are of great interest. We have introduced an algorithm that in the absence of direct connections, searches for indirect pathways that use other connected structures as relays.

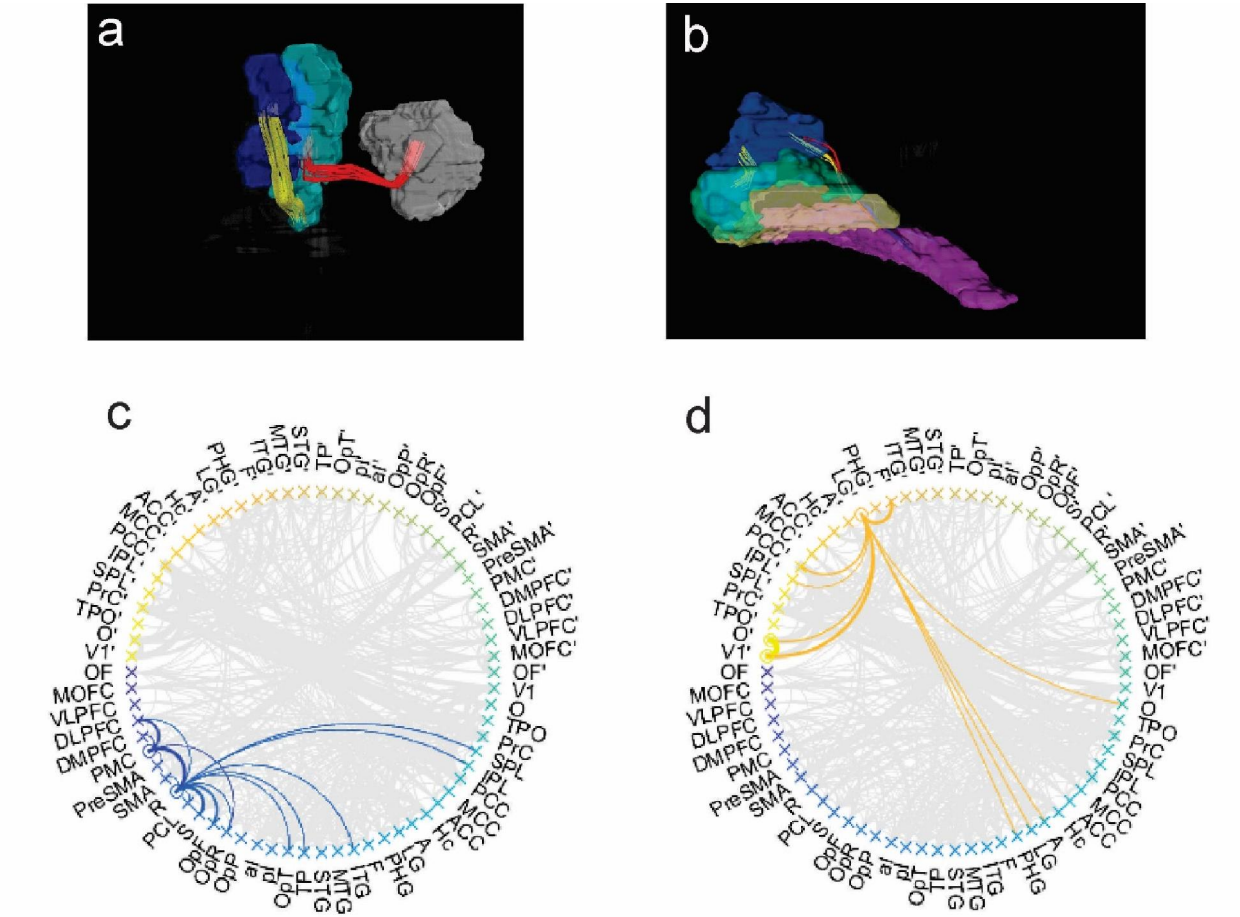

Figure 12. Sample propagation pathways. a,c) the horizontal part of superior longitudinal fascicle (PMC → R → IPL) in 3D fiber (a) and circular representation (c); b,d) ventral stream (V1'→O'→LG'→F') in 3D fiber (b) and circular representation (d).

Structural-Effective Connectome

Conclusions

- The work presented here provides a method to obtain a whole-brain connectome, applied to physiological connections.
- Using the same method, a population-based “pathological” connectome, comprised of connections between structures belonging to the epileptogenic zone could possibly be created whenever a significant number of patients for each different pathology are going to be investigated.
- Comparing a physiological with a pathological connectome, we can quantify the plasticity focal epilepsy promotes in human neuronal networks and ideally utilize it for diagnostic and prognostic purposes.

Acknowledgments

We would like to thank Alin Rasina, MD, Bogdan Balanescu, MD, Ana Ciurea, MD for their contribution to the surgical procedures and to Mihai Maliia, MD, Irina Popa, MD, Sabina Ene, BSc, for their contribution to the presurgical evaluation of the patients and data collection. This work was supported by Romanian government UEFISCDI research grant PN-II-IDPCE-2011-3-0240.

References

Andrei Barborica, Cristian Donos, Ioana Mindruta, Jean Ciurea. Time-locking of single-unit activity to electrical stimulation: a possible signature of human epileptogenic cortex, presented at International Conference Brain States: Characterization And Neuromodulation by DBS, Koln, Germany, November 11-13, 2015.

Donos C, Mălîia MD, Mîndruţă I, Popa I, Ene M, Bălănescu B, Ciurea A, Barborica A. A connectomics approach combining structural and effective connectivity assessed by intracranial electrical stimulation. Neuroimage. 2016a; 132:344-58. doi: 10.1016/j.neuroimage.2016.02.054

Donos C, Mîndruţă I, Ciurea J, Mălîia MD, Barborica A. A comparative study of the effects of pulse parameters for intracranial direct electrical stimulation in epilepsy. Clin Neurophysiol. 2016b;127(1):91-101. doi: 10.1016/j.clinph.2015.02.013.